Asociación Argentina
de Mecánica Computacional

Mecánica Computacional Vol XXVI, pp.1104-1119
Sergio A. Elaskar, Elvio A. Pilotta, Germán A. Torres (Eds.)
Córdoba, Argentina, Octubre 2007

BEM FOR THE ANALYSIS OF FLUID FLOW AROUND MEMS

Víctor D. Fachinotti[a], Alberto Cardona[a], Jorge D'Elía[a] and Stéphane Paquay[b]

[a]*Centro Internacional de Métodos Computacionales en Ingeniería (CIMEC-INTEC) – Universidad Nacional del Litoral (UNL) / Consejo Nacional de Investigaciones Científicas y Técnicas (CONICET) – Güemes 3450, S3000GLN Santa Fe, Argentina – E-mails: vfachino@intec.unl.edu.ar, acardona@intec.unl.edu.ar, jdelia@intec.unl.edu.ar, http://www.intec.unl.edu.ar*
[b]*Open Engineering SA – Rue des Chasseurs Ardennais, 8, B-4031 Angleur, Belgium – E-mail: s.paquay@open-engineering.com, http://www.open-engineering.com*

Keywords: MEMS, Boundary Element Method, Stokes, incompressible.

Abstract. The boundary element method (BEM) is used in this work for modelling the fluid flow around a vibrating micro-electro-mechanical system (MEMS). Device motion induces flow and, therefore, drag-forces develop on the surface of the MEMS with a damping effect on the MEMS vibration. We assume that the fluid around MEMS can be treated as a continuum and, further on, that the flow can be modelled as incompressible with a very low Reynolds number. Under such conditions, met in a large number of MEMS in practice, the fluid flow can be accurately described by Stokes theory of quasi-steady incompressible flow. We take into account MEMS deformation effects on fluid flow analysis.

Fast integration is performed using the collocation method. Self-integrals containing singular kernels are analytically computed over linear triangles.

This model has been computationally implemented into the engineering software OOFELIE:MEMS, developed by Open Engineering SA.

The accuracy of the model is tested using a benchmark problem – the flow around a sphere moving with constant velocity–, with satisfactory results. Preliminary results of an application to MEMS are also shown.

1 INTRODUCTION

Micro-Electro-Mechanical Systems (MEMS) consist of fixed or moving micro-structures playing the role of actuators or sensors in many advanced applications. Typical MEMS are arrays of beams or plates where the thickness is $O(1\mu\text{m})$ and the length is $O(10\mu\text{m} - 1\text{mm})$. MEMS motion or deformation can be induced by mechanical, electrical, thermal, acoustical or photonic energy sources.

In this work, we are particularly interested in vibrating MEMS immersed in a fluid (typically, air) environment. The aim is to determine the drag forces induced in the MEMS surface by the fluid flowing around. Such forces have a damping effect on MEMS vibration.

The problem of MEMS vibration in a fluid media will be assumed to be governed by the quasi-steady incompressible Stokes equation. This approach is valid for MEMS under the following hypotheses:

- the frequency of vibration is low enough to turn inertia forces negligible compared to viscous forces,
- the fluid around MEMS is assumed to behave as a continuum, and hence the fluid, even a gas, is modelled as incompressible.

The previous hypotheses hold in a large number of MEMS in practice (Mukherjee et al., 2005; Frangi and Tausch, 2005; Frangi and Di Gioia, 2005; Frangi et al., 2006; Wang et al., 2006). The first hypothesis is verified when the typical length of the MEMS device is smaller that the penetration length, which depends on the vibration frequency and the fluid density. The second hypothesis holds for gases when the Knudsen number *Kn*, that is the ratio of the mean free path of the gas molecule to the characteristic length of the flow, does not exceed 0.001 (Ding and Ye, 2004).

Continuum hypothesis is closely linked to the non-slip condition at the surface of the MEMS, only valid for slightly rarified gases. Recently, Ding and Ye (2004) and Frangi et al. (2006) developed boundary element methods that take into account the slip-flow regime, extending the validity of the continuum hypothesis to $Kn \leq 0.1$. In a preliminary approach, these effects will be neglected in the current work.

On the other hand, unlike the above-mentioned works assuming the MEMS to be rigid-bodies to the purpose of fluid analysis, we will take into account the effect of MEMS deformation on fluid flow.

It is usually assumed that in the case of deformable bodies, certain terms in the fluid flow computation can be neglected as if the body behaves as a rigid one (Kim and Karrila, 1991; Ding and Ye, 2004; Mukherjee et al., 2005; Frangi and Tausch, 2005; Frangi and Di Gioia, 2005; Frangi et al., 2006; Wang et al., 2006). For the sake of generality, the effect of MEMS deformation on fluid flow will be accounted for in this work.

The current model is available into the software OOFELIE::MEMS, a virtual prototyping tool for the analysis and design of MEMS developed by Open Engineering SA.

The outline of the paper is as follows. In Section 2, the Stokes equations for incompressible steady flow are derived, together with its fundamental solution and the Green identity that constitute the base of the boundary integral formulation of Stokes equations. Sections 3 and 4 are devoted to the integral representation of interior and exterior flow problems, respectively, considering points located either inside or outside the flow domain, or at the interface. In Section 5, we develop a boundary element method to solve the exterior problem at boundary points, which is the problem we are particularly interested in. Section 6 describes the analytical integration of

singular integrals. Finally, in Section 7, the current model is applied to the classical benchmark of a sphere translating in a viscous fluid, as well as to simulate a vibrating beam in a MEMS.

2 BEM STOKES EQUATIONS

The flow of an incompressible Newtonian fluid in a domain Ω is governed by the following equations:

$$\frac{\partial V_i}{\partial x_i} = 0, \qquad \text{mass balance (or continuity) equation,} \tag{1}$$

$$\rho\left(\frac{\partial V_i}{\partial t} + u_j\frac{\partial V_i}{\partial x_j}\right) = F_i + \frac{\partial \sigma_{ij}}{\partial x_j}, \qquad \text{momentum balance equation,} \tag{2}$$

$$\sigma_{ij} = \mu\left(\frac{\partial V_i}{\partial x_j} + \frac{\partial V_j}{\partial x_i}\right) - P\delta_{ij}, \qquad \text{constitutive equation,} \tag{3}$$

where V_i is the velocity, σ_{ij} is the stress tensor, P is the pressure, ρ is the fluid density, μ is the dynamic viscosity of the fluid, F_i is the body force per unit mass, δ_{ij} is the Kronecker delta ($\delta_{ij} = 1$ if $i = j$, $\delta_{ij} = 0$ if $i \neq j$), x_i is the Cartesian coordinate along the i-axis, and t is the time.

We will next linearize the equations of fluid motion. Let us assume that the velocity field $\mathbf{V}$ and the pressure field P can be expressed as the sum of small perturbations with respect to reference states $\mathbf{V}_0$ and P_0 respectively, i.e.:

$$P = P_0 + p, \qquad \mathbf{V} = \mathbf{V}_0 + \mathbf{v}.$$

We assume further that the fluid is at rest at the reference state ($\mathbf{V}_0 = \mathbf{0}$, $P_0 = \text{const}$). Then, the continuity equation (1) reduces to

$$\frac{\partial v_i}{\partial x_i} = 0, \tag{4}$$

and by considering the constitutive law (3), the last term of the r.h.s. of the momentum equation (2) takes the form

$$\frac{\partial \sigma_{ij}}{\partial x_j} = -\frac{\partial P}{\partial x_i} + \mu\frac{\partial^2 v_i}{\partial x_j \partial x_j} = -\frac{\partial p}{\partial x_i} + \mu\frac{\partial^2 v_i}{\partial x_j \partial x_j}. \tag{5}$$

Then, in the case of negligible body forces ($F_i = 0$), the momentum equation (2) can be expressed as

$$\rho\left(\frac{\partial v_i}{\partial t} + v_j\frac{\partial v_i}{\partial x_j}\right) = -\frac{\partial p}{\partial x_i} + \mu\frac{\partial^2 v_i}{\partial x_j \partial x_j}.$$

Finally, the hypothesis of small perturbations allows us to ignore the second-order term in the above equation, obtaining:

$$\rho\frac{\partial v_i}{\partial t} + \frac{\partial p}{\partial x_i} - \mu\frac{\partial^2 v_i}{\partial x_j \partial x_j} = 0, \tag{6}$$

which, together with the incompressibility condition (4), constitute the *unsteady (linearized) Stokes equations*.

A last simplification consists of considering the inertia forces negligible compared to viscous forces. This assumption can usually be made in MEMS applications for frequencies below 100Hz (Mukherjee et al., 2005; Frangi and Tausch, 2005; Frangi and Di Gioia, 2005; Frangi et al., 2006; Wang et al., 2006). This yields the *quasi-steady (linearized) Stokes equations* that can be written as:

$$\frac{\partial v_i}{\partial x_i} = 0 \tag{7}$$

$$\frac{\partial p}{\partial x_i} - \mu \frac{\partial^2 v_i}{\partial x_j \partial x_j} = 0. \tag{8}$$

2.1 Fundamental solution

Let us consider the quasi-steady Stokes problem:

$$\begin{aligned} &\frac{\partial v_i}{\partial x_i} = 0, \\ &\frac{\partial p}{\partial x_i} - \mu \frac{\partial^2 v_i}{\partial x_j \partial x_j} = g_i \delta(\mathbf{x} - \mathbf{y}) \qquad\qquad \forall \mathbf{x}, \mathbf{y} \in \mathbb{R}^3, \end{aligned}$$

where δ is the Dirac delta function, such that the force g_i is concentrated at point $\mathbf{y}$ (the "load" or "source" point). The solution of this problem –the so-called fundamental solution– can be expressed as (Kim and Karrila, 1991):

$$\begin{aligned} v_i(\mathbf{x}) &= G_{ij}(\mathbf{x}, \mathbf{y}) g_j, \\ p(\mathbf{x}) &= H_i(\mathbf{x}, \mathbf{y}) g_i, \end{aligned}$$

where G_{ij} and H_i are the kernels defined as:

$$G_{ij}(\mathbf{x}, \mathbf{y}) = \frac{1}{8\pi\mu} \left(\frac{\delta_{ij}}{r} + \frac{r_i r_j}{r^3} \right), \tag{9}$$

$$H_i(\mathbf{x}, \mathbf{y}) = \frac{1}{4\pi} \frac{r_i}{r^3}, \tag{10}$$

with $\mathbf{r} = \mathbf{x} - \mathbf{y}$ and $r = \|\mathbf{r}\|$. The kernel G_{ij} is known as "Stokeslet", and can be derived from the Kelvin kernel for elasticity

$$G^e_{ij} = \frac{1}{16\pi(1-\nu)\mu} \left[(3 - 4\nu) \frac{\delta_{ij}}{r} + \frac{r_i r_j}{r^3} \right] \tag{11}$$

when the Poisson ratio ν equals 0.5 (incompressible case).

2.2 Green identity

Given a velocity field $\mathbf{u}$ and a pressure field q, the stress $\sigma_{ij}(\mathbf{u}, q)$ is given by the expression:

$$\sigma_{ij}(\mathbf{u}, q) = -q\delta_{ij} + \mu \left(\frac{\partial u_i}{\partial x_j} + \frac{\partial u_j}{\partial x_i} \right).$$

Then, the following identity holds:

$$\begin{aligned}\frac{\partial}{\partial x_j}\left(\sigma_{ij}\left(\mathbf{u},q\right)v_i\right) &= \frac{\partial \sigma_{ij}}{\partial x_j}v_i + \sigma_{ij}\frac{\partial v_i}{\partial x_j} \\ &= \left(-\frac{\partial q}{\partial x_i} + \mu\frac{\partial^2 u_i}{\partial x_j \partial x_j}\right)v_i + \mu\left(\frac{\partial u_i}{\partial x_j} + \frac{\partial u_j}{\partial x_i}\right)\frac{\partial v_i}{\partial x_j} \\ &= \left(-\frac{\partial q}{\partial x_i} + \mu\frac{\partial^2 u_i}{\partial x_j \partial x_j}\right)v_i + \frac{\mu}{2}\left(\frac{\partial u_i}{\partial x_j} + \frac{\partial u_j}{\partial x_i}\right)\left(\frac{\partial v_i}{\partial x_j} + \frac{\partial v_j}{\partial x_i}\right).\end{aligned}$$

By integration on the domain Ω and after applying the Gauss theorem, we get the so-called Green's first formula (Power and Wrobel, 1995):

$$\int_\Omega \left(\frac{\partial q}{\partial y_i} - \mu\frac{\partial^2 u_i}{\partial y_j \partial y_j}\right)v_i \,\mathrm{d}\Omega_y = \frac{\mu}{2}\int_\Omega \left(\frac{\partial u_i}{\partial y_j} + \frac{\partial u_j}{\partial y_i}\right)\left(\frac{\partial v_i}{\partial y_j} + \frac{\partial v_j}{\partial y_i}\right)\mathrm{d}\Omega_y - \int_\Sigma \sigma_{ij}\left(\mathbf{u},q\right)v_i n_j \,\mathrm{d}\Sigma_y, \quad (12)$$

where **n** is the unit vector normal to Σ pointing outwards Ω, as shown in Figure 1.

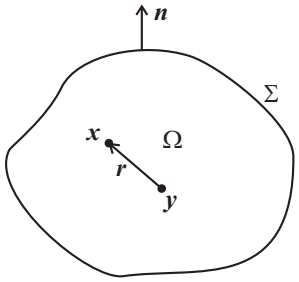

Figure 1: Domain for the analysis of interior Stokes flow.

3 DIRECT INTEGRAL REPRESENTATION FOR INTERIOR PROBLEM

For **g** given by the canonic unit vector in the k-direction, i.e. $g_j = \delta_{kj}$, it can be verified that

$$\frac{\partial H_m}{\partial x_k} - \mu\frac{\partial^2 G_{mk}}{\partial x_j \partial x_j} = \delta_{km}\delta(\mathbf{x}-\mathbf{y}).$$

First, let us multiply the above equation by v_k and then integrate over the domain Ω:

$$\int_\Omega \left(\frac{\partial H_m}{\partial y_k} - \mu\frac{\partial^2 G_{mk}}{\partial y_j \partial y_j}\right)v_k \,\mathrm{d}\Omega_y = \int_\Omega v_m \delta(\mathbf{x}-\mathbf{y})\,\mathrm{d}\Omega_y.$$

Using the definition of Dirac function, the right-hand side of the last equation becomes

$$\int_\Omega v_m(\mathbf{y})\delta(\mathbf{x}-\mathbf{y})\,\mathrm{d}\Omega_y = \alpha(\mathbf{x})v_m(\mathbf{x}),$$

where

$$\alpha(\mathbf{x}) = \begin{cases} 1 & \text{if } \mathbf{x} \in \Omega, \\ 0 & \text{if } \mathbf{x} \notin \bar{\Omega}, \end{cases}$$

being $\bar{\Omega} = \Omega \cup \Sigma$ the closure of the (open) domain Ω.

By now using the Green identity (12), we obtain:

$$\alpha(\mathbf{x})v_m(\mathbf{x}) = \int_\Omega \frac{\mu}{2}\left(\frac{\partial G_{mk}}{\partial y_j} + \frac{\partial G_{jm}}{\partial y_k}\right)\left(\frac{\partial v_k}{\partial y_j} + \frac{\partial v_j}{\partial y_k}\right) \mathrm{d}\Omega_y - \int_\Sigma S_{mk} v_k \,\mathrm{d}\Sigma_y, \tag{13}$$

where S_{mk} is the "tractionlet" kernel:

$$S_{mk}(\mathbf{x},\mathbf{y}) = R_{kjm}(\mathbf{x},\mathbf{y})n_j(\mathbf{y}), \tag{14}$$

and R_{kjm} the "stresslet" kernel:

$$R_{kjm}(\mathbf{x},\mathbf{y}) = -H_m\delta_{kj} + \mu\left(\frac{\partial G_{mk}}{\partial x_j} + \frac{\partial G_{jm}}{\partial x_k}\right) = -\frac{3}{4\pi}\frac{r_k r_j r_m}{r^5}. \tag{15}$$

Secondly, we multiply the momentum equation (8) by G_{mk} and integrate over Ω:

$$\int_\Omega \left(\frac{\partial p}{\partial y_k} - \mu\frac{\partial^2 v_k}{\partial y_i \partial y_i}\right) G_{mk} \,\mathrm{d}\Omega_y = 0.$$

After applying the Green identity (12), we get:

$$\int_\Omega \frac{\mu}{2}\left(\frac{\partial G_{mk}}{\partial y_j} + \frac{\partial G_{jm}}{\partial y_k}\right)\left(\frac{\partial v_k}{\partial y_j} + \frac{\partial v_j}{\partial y_k}\right) \mathrm{d}\Omega_y - \int_\Sigma \sigma_{kj}\left(\mathbf{v},p\right) G_{mk} n_j \,\mathrm{d}\Sigma_y = 0. \tag{16}$$

Finally, subtracting equation (16) from equation (13), we get the boundary integral equation for the velocity field in the interior of Ω:

$$\alpha(\mathbf{x})v_m(\mathbf{x}) = \int_\Sigma G_{mk}\sigma_{kj}\left(\mathbf{v},p\right) n_j \,\mathrm{d}\Sigma_y - \int_\Sigma S_{mk} v_k \,\mathrm{d}\Sigma_y. \tag{17}$$

3.1 Interior problem on the boundary

The boundary integral equation (17) becomes singular for points located at the boundary. To avoid this singularity, let us replace Ω in equation (17) by $\Omega \cup S_\varepsilon$, being S_ϵ a portion of a little sphere of radius ε and center $\mathbf{x} \in \Sigma$, as shown in Figure 2. Then, the boundary integral expression of an interior Stokes problem at the boundary points $\mathbf{x} \in \Sigma$ can be obtained by taking the limit of the equation (17) for interior points when $\varepsilon \to 0$:

$$v_m(\mathbf{x}) = \lim_{\varepsilon\to 0}\Bigg[\int_{\Sigma-\partial S_i} G_{mk}\sigma_{kj}\left(\mathbf{v},p\right) n_j \,\mathrm{d}\Sigma_y - \int_{\Sigma-\partial S_i} S_{mk} v_k \,\mathrm{d}\Sigma_y + \int_{\partial S_e} G_{mk}\sigma_{kj}\left(\mathbf{v},p\right) n_j \,\mathrm{d}\Sigma_y - \int_{\partial S_e} S_{mk} v_k \,\mathrm{d}\Sigma_y\Bigg], \tag{18}$$

where ∂S_i is the interface between Ω and S_ε, and ∂S_e is the remainder portion of the boundary of S_ε (see Figure 2). The limit as $\varepsilon \to 0$ of the integral over $\Sigma - \partial S_i$ is the integral over Σ in the sense of the Cauchy Principal Value (CPV) (París and Cañas, 1997), denoted as:

$$⨍_\Sigma f(\mathbf{y}) \,\mathrm{d}\Sigma_y = \lim_{\varepsilon\to 0}\int_{\Sigma-\partial S_i} f(\mathbf{y}) \,\mathrm{d}\Sigma_y. \tag{19}$$

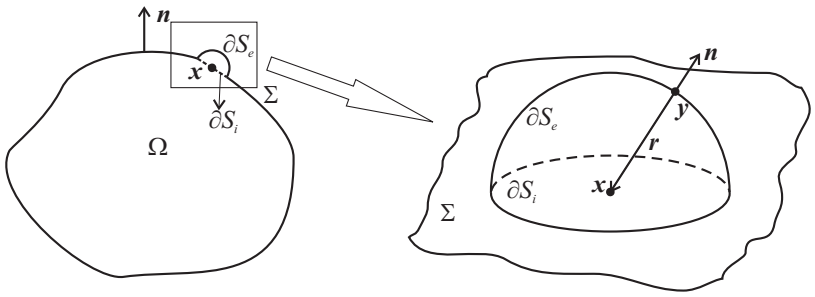

Figure 2: Domain for the analysis of interior Stokes flow at boundary points.

Since $\mathbf{v}$ and $\boldsymbol{\sigma}$ are continuous fields, $\mathbf{v} \to \mathbf{v}(\mathbf{x})$ and $\boldsymbol{\sigma} \to \boldsymbol{\sigma}(\mathbf{x})$ as $\varepsilon \to 0$, then

$$C^{-}_{mk}(\mathbf{x})v_k(\mathbf{x}) = \fint_{\Sigma} G_{mk}\sigma_{kj}\left(\mathbf{v}, p\right) n_j \, \mathrm{d}\Sigma_y - \fint_{\Sigma} S_{mk} v_k \, \mathrm{d}\Sigma_y + \left(\lim_{\varepsilon \to 0} \int_{\partial S_e} G_{mk} n_j \, \mathrm{d}\Sigma_y\right) \sigma_{kj}(\mathbf{x}), \tag{20}$$

where

$$C^{-}_{mk}(\mathbf{x}) = \delta_{mk} + \lim_{\varepsilon \to 0} \int_{\partial S_e} S_{mk} \, \mathrm{d}\Sigma_y. \tag{21}$$

Given the normal unit vector pointing outwards ∂S_e by $n_j = -r_j/\varepsilon$ (see Figure 2), we realize that

$$\int_{\partial S_e} G_{mk} n_j \, \mathrm{d}\Sigma_y = -\frac{1}{8\pi\mu} \int_{\partial S_e} \left(\frac{\delta_{km}}{\varepsilon} + \frac{r_k r_m}{\varepsilon^3}\right) \frac{r_j}{\varepsilon} \, \mathrm{d}\Sigma_y = O(\varepsilon),$$

and therefore

$$\lim_{\varepsilon \to 0} \int_{\partial S_e} G_{mk} n_j \, \mathrm{d}\Sigma_y = 0.$$

This is not the case for the integral

$$\int_{\partial S_e} S_{mk} \, \mathrm{d}\Sigma_y = \frac{3}{4\pi} \int_{\partial S_e} \frac{r_k r_m}{\varepsilon^4} \, \mathrm{d}\Sigma_y = O(1), \tag{22}$$

whose limit is computed below regarding the shape of the surface at $\mathbf{x}$.

3.1.1 Smooth surface

When Σ is smooth at the vicinity of $\mathbf{x}$, i.e. it exists a tangent plane at $\mathbf{x}$, ∂S_e can be assimilated to a hemispheric surface as $\varepsilon \to 0$. This yields (Power and Wrobel, 1995)

$$\lim_{\varepsilon \to 0} \int_{\partial S_e} S_{mk} \, \mathrm{d}\Sigma_y = -\frac{1}{2}\delta_{mk}, \tag{23}$$

and hence

$$C^{-}_{mk}(\mathbf{x}) = \frac{1}{2}\delta_{mk}. \tag{24}$$

Therefore, when the surface is smooth at the vicinity of $\mathbf{x} \in \Sigma$, the boundary integral equation describing interior Stokes flow at this point takes the form:

$$\frac{1}{2}v_m(\mathbf{x}) = \fint_{\Sigma} G_{mk}\sigma_{kj}\left(\mathbf{v}, p\right) n_j \, \mathrm{d}\Sigma_y - \fint_{\Sigma} S_{mk} v_k \, \mathrm{d}\Sigma_y. \tag{25}$$

3.1.2 Non-smooth surface

Invoking the definition of the Cauchy Principal Value given by equation (19), we can write

$$\lim_{\varepsilon \to 0} \int_{\partial S_e} S_{mk} \, \mathrm{d}\Sigma_y = \int_{\Sigma} S_{mk} \, \mathrm{d}\Sigma_y - \fint_{\Sigma} S_{mk} \, \mathrm{d}\Sigma_y. \tag{26}$$

Considering an interior point $\mathbf{x} \in \Omega$, we know after Power and Wrobel (1995) that

$$\int_{\Sigma} S_{mk} \, \mathrm{d}\Sigma_y = -\delta_{mk}. \tag{27}$$

Then, $C^{-}_{mk}(\mathbf{x})$ can be expressed as

$$C^{-}_{mk}(\mathbf{x}) = -\fint_{\Sigma} S_{mk} \, \mathrm{d}\Sigma_y. \tag{28}$$

So, if the surface is not smooth in the neighborhood of $\mathbf{x} \in \Sigma$, the interior Stokes flow at this point obeys the boundary integral equation

$$\left(-\fint_{\Sigma} S_{mk} \, \mathrm{d}\Sigma_y \right) v_m(\mathbf{x}) = \fint_{\Sigma} G_{mk} \sigma_{kj} \left(\mathbf{v}, p \right) n_j \, \mathrm{d}\Sigma_y - \fint_{\Sigma} S_{mk} v_k \, \mathrm{d}\Sigma_y. \tag{29}$$

4 DIRECT INTEGRAL REPRESENTATION FOR THE EXTERIOR PROBLEM

Let Ω be now a structure (e.g., a MEMS) surrounded by a domain Ω' containing a fluid medium, as shown in Figure 3. The boundary of Ω' is composed of the internal surface Σ (boundary of Ω) and the external surface S_∞. The formulation developed in the previous section for interior problems is still valid when applied to the domain Ω':

$$\alpha'(\mathbf{x}) v_m(\mathbf{x}) = \int_{\Sigma \cup S_\infty} G_{mk} \sigma_{kj} \left(\mathbf{v}, p \right) n'_j \, \mathrm{d}\Sigma_y - \int_{\Sigma \cup S_\infty} R_{kjm} v_k n'_j \, \mathrm{d}\Sigma_y,$$

where

$$\alpha'(\mathbf{x}) = \left\{ \begin{array}{ll} 1 & \text{if } \mathbf{x} \in \Omega' \\ 0 & \text{if } \mathbf{x} \notin \bar{\Omega}' \end{array} \right\} = 1 - \alpha, \tag{30}$$

and $\mathbf{n}'$ is the unit vector normal to the surface of Ω' (either Σ or S_∞), pointing outwards Ω'. At the surface Σ, $\mathbf{n}'$ is opposite to the previously defined normal $\mathbf{n}$ pointing outwards the structure Ω.

Furthermore, when Ω' becomes infinitely large (for a given fixed structure Ω), contributions coming from S_∞ become infinitely small and we get:

$$\left[1 - \alpha(\mathbf{x}) \right] v_m(\mathbf{x}) = \int_{\Sigma} S_{mk} v_k \, \mathrm{d}\Sigma_y - \int_{\Sigma} G_{mk} \sigma_{kj} \left(\mathbf{v}, p \right) n_j \, \mathrm{d}\Sigma_y. \tag{31}$$

4.1 Exterior problem on the boundary

Using a procedure analogous to that described in Section 3.1, the extension of equation (31) to points $\mathbf{x} \in \Sigma$ takes the form

$$C_{mk}(\mathbf{x}) v_k(\mathbf{x}) = \fint_{\Sigma} S_{mk} v_k \, \mathrm{d}\Sigma_y - \fint_{\Sigma} G_{mk} \sigma_{kj} \left(\mathbf{v}, p \right) n_j \, \mathrm{d}\Sigma_y, \tag{32}$$

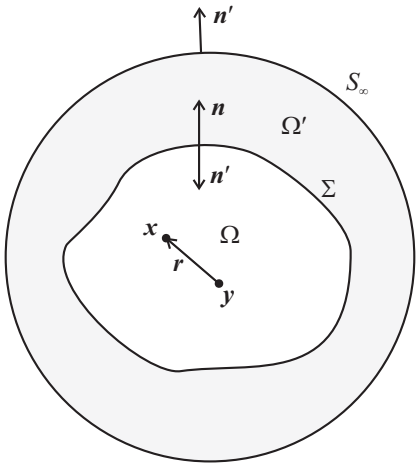

Figure 3: Domain for the analysis of exterior Stokes flow.

with

$$C_{mk} = \delta_{mk} - C^{-}_{mk}(\mathbf{x}). \tag{33}$$

If the surface in the vicinity of $\mathbf{x} \in \Sigma$ is smooth, we take C^{-}_{mk} as defined by equation (24), obtaining have

$$\frac{1}{2} v_m(\mathbf{x}) = \fint_{\Sigma} S_{mk} v_k \, \mathrm{d}\Sigma_y - \fint_{\Sigma} G_{mk} \sigma_{kj}\left(\mathbf{v}, p\right) n_j \, \mathrm{d}\Sigma_y. \tag{34}$$

Otherwise, we use C^{-}_{mk} defined by equation (28) in case of non-smooth boundary in the vicinity of $\mathbf{x} \in \Sigma$ to write:

$$\left(\delta_{mk} + \fint_{\Sigma} S_{mk} \, \mathrm{d}\Sigma_y\right) v_k(\mathbf{x}) = \fint_{\Sigma} S_{mk} v_k \, \mathrm{d}\Sigma_y - \fint_{\Sigma} G_{mk} \sigma_{kj}\left(\mathbf{v}, p\right) n_j \, \mathrm{d}\Sigma_y. \tag{35}$$

4.2 Fluid/solid boundary conditions

Let Ω be a solid body immersed in a fluid environment Ω', such that Σ represents the fluid/solid interface. The stress vector (or traction) at this interface is given by

$$t_k = \sigma_{kj} n_j.$$

This vector can be computed in terms of the velocities at the boundary by solving the boundary integral equation (32), written now as:

$$C_{mk}(\mathbf{x}) v_k(\mathbf{x}) = \fint_{\Sigma} S_{mk} v_k \, \mathrm{d}\Sigma_y - \fint_{\Sigma} G_{mk} t_k \, \mathrm{d}\Sigma_y. \tag{36}$$

As aforementioned, we are particularly interested in determining the drag forces induced by an exterior flow on the surface Σ of the structure Ω. Such drag forces will play the role of damping forces in the analysis of vibrations in the solid structure. For exterior Stokes problems, $\mathbf{t}$ represents the force per unit area exerted by the solid on the liquid through the interface Σ, so that the drag force (action of the liquid onto the solid) per unit area we are looking for is given by $\tilde{\mathbf{t}} = -\mathbf{t}$. Using $\tilde{\mathbf{t}}$ instead of $\mathbf{t}$, the previous equation takes the form

$$C_{mk}(\mathbf{x}) v_k(\mathbf{x}) = \fint_{\Sigma} S_{mk} v_k \, \mathrm{d}\Sigma_y + \fint_{\Sigma} G_{mk} \tilde{t}_k \, \mathrm{d}\Sigma_y. \tag{37}$$

5 BEM DISCRETIZATION

The boundary integral equation (37) will be discretized using the boundary element method. To this end, the surface Σ is approximated using a mesh of linear triangular finite elements. Then, the velocity and the drag force per unit area are approximated in the standard (Galerkin) way:

$$\mathbf{v}(\mathbf{x}) = \mathbf{N}_J(\mathbf{x})\mathbf{V}_J,$$
$$\tilde{\mathbf{t}}(\mathbf{x}) = \mathbf{N}_J(\mathbf{x})\mathbf{T}_J,$$

where $\mathbf{N}_J$ is the shape function associated to node J and $\mathbf{V}_J$ and $\mathbf{T}_J$ the approximations to the velocity and drag force per unit area, respectively, at this point. In 3D applications, $\mathbf{N}_j$ is the diagonal matrix:

$$\mathbf{N}_J(\mathbf{x}) = N_J(\mathbf{x})\mathbf{I},$$

where N_J is the scalar shape function associated to node J, such that $N_J(\mathbf{x}_I) = \delta_{IJ}$.

Introducing these approximations into equation (37), we obtain

$$\left[\mathbf{C}(\mathbf{x})\mathbf{N}_J(\mathbf{x}) - \fint_\Sigma \mathbf{S}(\mathbf{x},\mathbf{y})\mathbf{N}_J(\mathbf{y})\,\mathrm{d}\Sigma_y\,\mathrm{d}\Sigma_x\right]\mathbf{V}_J = \left[\fint_\Sigma \mathbf{G}(\mathbf{x},\mathbf{y})\mathbf{N}_J(\mathbf{y})\,\mathrm{d}\Sigma_y\,\mathrm{d}\Sigma_x\right]\mathbf{T}_J. \tag{38}$$

5.1 Collocation discretization

The collocation method consists of enforcing the discretized boundary integral equation (38) to hold at certain points called collocation points. Here, we adopt as collocation points the nodal points $\mathbf{x}_I \in \Sigma$ ($I = 1, 2, \ldots, N$). At each collocation point, the following linear system is obtained:

$$\mathbf{A}_{IJ}\mathbf{V}_J = \mathbf{B}_{IJ}\mathbf{T}_J, \tag{39}$$

with

$$\mathbf{A}_{IJ} = \mathbf{C}(\mathbf{x}_I)\delta_{IJ} - \fint_\Sigma \mathbf{S}(\mathbf{x}_I,\mathbf{y})\mathbf{N}_J(\mathbf{y})\,\mathrm{d}\Sigma_y, \tag{40}$$

$$\mathbf{B}_{IJ} = \fint_\Sigma \mathbf{G}(\mathbf{x}_I,\mathbf{y})\mathbf{N}_J(\mathbf{y})\,\mathrm{d}\Sigma_y. \tag{41}$$

Once the surface Σ has been discretized into M boundary elements Σ_e, the integrals in the above equation can be computed by summing the contributions from every boundary element:

$$\fint_\Sigma f(\mathbf{x}_I,\mathbf{y})\,\mathrm{d}\Sigma_y = \sum_{e=1}^{M}\fint_{\Sigma_e} f(\mathbf{x}_I,\mathbf{y})\,\mathrm{d}\Sigma_y = \sum_{e=1}^{S}\fint_{\Sigma_e} f(\mathbf{x}_I,\mathbf{y})\,\mathrm{d}\Sigma_y + \sum_{e=S+1}^{M}\int_{\Sigma_e} f(\mathbf{x}_I,\mathbf{y})\,\mathrm{d}\Sigma_y.$$

Let us notice that the integrals over those elements $\Sigma_1, \Sigma_2, \ldots, \Sigma_S$ containing the collocation point $\mathbf{x}_I$ exist only in the sense of CPV and can not be computed using standard quadrature rules. Over the remainder elements $\Sigma_{S+1}, \ldots, \Sigma_M$, standard numerical quadrature is used.

6 COMPUTATION OF SINGULAR INTEGRALS

Let $\Sigma_e \equiv P_1$ be a linear triangle with vertex nodes $1, 2, 3$. Let us assume that one of these nodes, say node 1, coincides with the collocation point I. Looking at both kernels (9) and (15), we realize that $\mathbf{G}(\mathbf{x}_1, \mathbf{y})$ and $\mathbf{S}(\mathbf{x}_1, \mathbf{y})$ tends to infinity as $\mathbf{y} \to \mathbf{x}_1$. Such singular kernels require special treatment.

The integral involving $\mathbf{S}$ is null over the linear (then flat) triangle containing the collocation point. To demonstrate this, we realize that the position vector $\mathbf{r} = \mathbf{x}_1 - \mathbf{y}$ is orthogonal to the surface normal $\mathbf{n}$ throughout such element, such that $r_i n_i = 0$ at every point inside the element. Then,

$$S_{ij}(\mathbf{x}_I, \mathbf{y}) = R_{ijk} n_k = -\frac{3}{4\pi} \frac{r_i r_j}{r^5} r_k n_k = 0 \qquad \forall \mathbf{y} \in P_1. \tag{42}$$

Let us focus then on the integral containing $\mathbf{G}$:

$$B_{IJ_{mn}} = \fint_{P_1} G_{mn}(\mathbf{x}_I, \mathbf{y}) N_i(\mathbf{y}) \, \mathrm{d}\Sigma_y = \frac{1}{8\pi\mu} \left(D_{mnJ} + F_{mnJ} \right), \tag{43}$$

where

$$D_{mnJ} = \delta_{mn} \fint_{P_1} \frac{N_J}{r} \, \mathrm{d}\Sigma_y, \tag{44}$$

$$F_{mnJ} = \fint_{P_1} \frac{r_m r_n}{r^3} N_J \, \mathrm{d}\Sigma_y. \tag{45}$$

6.1 Change of coordinates

If ξ, η are the natural coordinates of the triangle P_1, with origin at the collocation point $\mathbf{x}_1$, we can write

$$N_1 = 1 - \xi - \eta, \qquad N_2 = \xi, \qquad N_3 = \eta.$$

Further, we define the transformation $(\xi, \eta) \to (r, \theta)$ as follows:

$$\xi = \frac{r}{c} \left(\frac{b}{h} \cos\theta - \sin\theta \right), \qquad \eta = \frac{r}{c} \left(-\frac{a}{h} \cos\theta + \sin\theta \right),$$

with r, θ, a, b, c and h defined in Figure 4.

Using this change of coordinates, every integral over P_1 can be computed as

$$\fint_{P_1} f(\xi, \eta) \, \mathrm{d}\Sigma_y = \int_{\theta_2}^{\theta_3} \int_0^{h/\cos\theta} f(\xi(r,\theta), \eta(r,\theta)) r \, \mathrm{d}r \, \mathrm{d}\theta. \tag{46}$$

6.2 Computation of D_{mni}

Using equation (46) we obtain:

$$I_{00} = \fint_{P_1} \frac{1}{r} \, \mathrm{d}\Sigma_y = \int_{\theta_2}^{\theta_3} \int_0^{h/\cos\theta} \mathrm{d}r \, \mathrm{d}\theta = h I_{\sec},$$

$$I_{10} = \fint_{P_1} \frac{\xi}{r} \, \mathrm{d}\Sigma_y = \int_{\theta_2}^{\theta_3} \int_0^{h/\cos\theta} \frac{1}{c} \left(\frac{b}{h} \cos\theta - \sin\theta \right) \mathrm{d}r \, \mathrm{d}\theta = \frac{bh}{2c} I_{\sec} - \frac{h^2}{2c} I_{\sec\tan},$$

$$I_{01} = \fint_{P_1} \frac{\eta}{r} \, \mathrm{d}\Sigma_y = \int_{\theta_2}^{\theta_3} \int_0^{h/\cos\theta} \frac{1}{c} \left(-\frac{a}{h} \cos\theta + \sin\theta \right) \mathrm{d}r \, \mathrm{d}\theta = -\frac{ah}{2c} I_{\sec} + \frac{h^2}{2c} I_{\sec\tan},$$

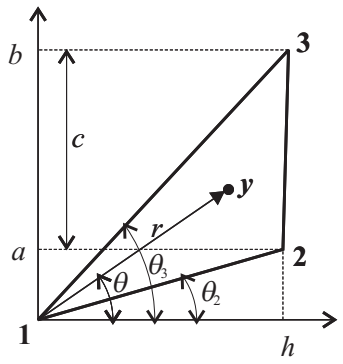

Figure 4: Parameters defining the coordinates transformation in a triangle.

where

$$I_{\sec} = \int_{\theta_2}^{\theta_3} \sec\theta \, \mathrm{d}\theta = \ln \frac{\sec\theta_3 + \tan\theta_3}{\sec\theta_2 + \tan\theta_2} = \ln \frac{d_{13} + b}{d_{12} + a},$$
$$I_{\sec\tan} = \int_{\theta_2}^{\theta_3} \sec\theta \tan\theta \, \mathrm{d}\theta = \sec\theta_3 - \sec\theta_2 = \frac{d_{13} - d_{12}}{h},$$

with $d_{ij} = \|\mathbf{x}_j - \mathbf{x}_i\|$ as the length of the side ij.

The term D_{mni} can be now computed for $i = 1, 2, 3$ as

$$D_{mn1} = \delta_{mn} I_{00} - D_{mn2} - D_{mn3}, \quad D_{mn2} = \delta_{mn} I_{10}, \quad D_{mn3} = \delta_{mn} I_{01}.$$

6.3 Computation of F_{mni}

First, let us realize that we can use the shape functions N_i to interpolate positions inside the element P_1 (as usually done with isoparametric finite elements):

$$r_m = \sum_{i=1}^{3} N_i(\xi, \eta) r_m^{(i)} = \xi r_m^{(2)} + \eta r_m^{(3)},$$

where $r_m^{(i)}$ is the i-th component of the position vector of node i, and we have assumed that the origin coincides with the position of node 1. This yields:

$$r_m r_n = r_m^{(2)} r_n^{(2)} \xi^2 + \left(r_m^{(2)} r_n^{(3)} + r_m^{(3)} r_n^{(2)} \right) \xi\eta + r_m^{(3)} r_n^{(3)} \eta^2.$$

Introducing this equation into the expression (45) for F_{mni}, we obtain

$$F_{mn1} = r_m^{(2)} r_n^{(2)} J_{20} + \left(r_m^{(2)} r_n^{(3)} + r_m^{(3)} r_n^{(2)} \right) J_{11} + r_m^{(3)} r_n^{(3)} J_{02} - F_{mn2} - F_{mn3},$$
$$F_{mn2} = r_m^{(2)} r_n^{(2)} J_{30} + \left(r_m^{(2)} r_n^{(3)} + r_m^{(3)} r_n^{(2)} \right) J_{21} + r_m^{(3)} r_n^{(3)} J_{12},$$
$$F_{mn3} = r_m^{(2)} r_n^{(2)} J_{21} + \left(r_m^{(2)} r_n^{(3)} + r_m^{(3)} r_n^{(2)} \right) J_{12} + r_m^{(3)} r_n^{(3)} J_{03},$$

being the integrals J_{ij}, computed in a way analogous to that employed in the previous section, defined as follows:

$$
\begin{aligned}
J_{11} &= \frac{h^2-ab}{hc^2}I_{\cos} + \frac{a+b}{c^2}I_{\sin} - \frac{h}{c^2}I_{\sec},\\
J_{20} &= \frac{b^2-h^2}{hc^2}I_{\cos} - 2\frac{b}{c^2}I_{\sin} + \frac{h}{c^2}I_{\sec},\\
J_{02} &= \frac{a^2-h^2}{hc^2}I_{\cos} - 2\frac{a}{c^2}I_{\sin} + \frac{h}{c^2}I_{\sec},\\
J_{21} &= \frac{h^2(a+2b)-ab^2}{2hc^3}I_{\cos} + \frac{2ab+b^2-h^2}{2c^3}I_{\sin} - \frac{h(a+2b)}{2c^3}I_{\sec} + \frac{h^2}{2c^3}I_{\sec\tan},\\
J_{12} &= \frac{a^2b-h^2(2a+b)}{2hc^3}I_{\cos} - \frac{a^2+2ab-h^2}{2c^3}I_{\sin} + \frac{h(2a+b)}{2c^3}I_{\sec} - \frac{h^2}{2c^3}I_{\sec\tan},\\
J_{30} &= \frac{b^3-3bh^2}{2hc^3}I_{\cos} - \frac{3b^2-h^2}{2c^3}I_{\sin} + \frac{3hb}{2c^3}I_{\sec} - \frac{h^2}{2c^3}I_{\sec\tan},\\
J_{03} &= \frac{3ah^2-a^3}{2hc^3}I_{\cos} + \frac{3a^2-h^2}{2c^3}I_{\sin} - \frac{3ha}{2c^3}I_{\sec} + \frac{h^2}{2c^3}I_{\sec\tan}.
\end{aligned}
$$

with

$$
\begin{aligned}
I_{\cos} &= \int_{\theta_2}^{\theta_3} \cos\theta\,\mathrm{d}\theta = \sin\theta_3 - \sin\theta_2 = \frac{b}{d_{13}} - \frac{a}{d_{12}},\\
I_{\sin} &= \int_{\theta_2}^{\theta_3} \sin\theta\,\mathrm{d}\theta = \cos\theta_2 - \cos\theta_3 = \frac{h}{d_{12}} - \frac{h}{d_{13}}.
\end{aligned}
$$

7 APPLICATIONS

7.1 Drag of a Stokes flow on a rigid sphere

In order to evaluate the accuracy of the model, it is applied to the classical benchmark of a rigid sphere translating with constant velocity $\mathbf{U}$ in a fluid with viscosity μ. The resultant of drag forces on the sphere is $F = 6\pi\mu R\|\mathbf{U}\|$. Some of the meshes of P_1 elements used for the analysis are shown in Figure 5.

Figure (6) shows the accuracy of the current model compared to that obtained by Frangi and Di Gioia (2005) using constant (P_0) triangles as a function of the number of degrees of freedom (d.o.f.).

The improvement of accuracy achieved with the current model thanks to the use of higher-order elements is quickly realized: note, for instance, that the error for the mesh of 3888 P_1 elements (1946 nodes, 5838 d.o.f.) is smaller than that obtained by Frangi and Di Gioia (2005) using a mesh of 12654 P_0 elements (37962 d.o.f.).

7.2 Drag on a vibrating MEMS

Let us consider the VIA vibrating beam accelerometer depicted in Figure 7 developed by the French aerospace laboratory ONERA (Le Traon et al., 1998; Masson, 2007). We are interested in determining the quality factor which is defined for a damped system as (Blom et al., 1992)

$$
Q = 2\pi\frac{\text{stored vibration energy}}{\text{dissipated energy per period}}. \tag{47}
$$

The part of the accelerometer that is the object of this study is the vibrating quartz beam highlighted in Figure 7. This beam is clamped at both ends, and its dimensions are: length $L = 2$

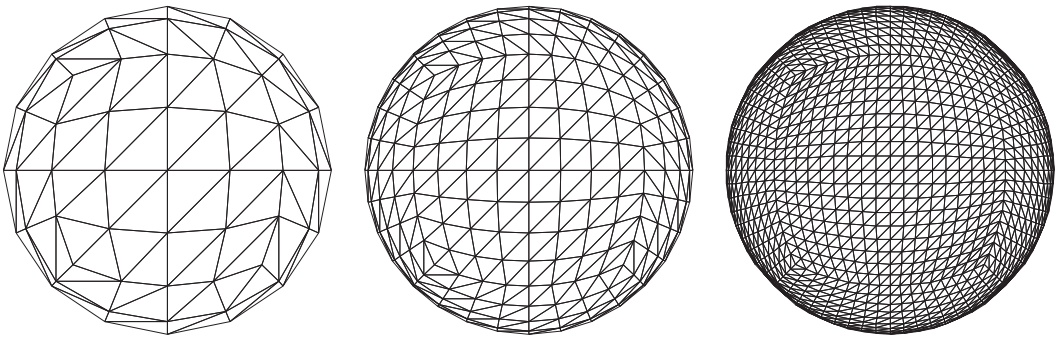

192 elements, 98 nodes 768 elements, 386 nodes 3888 elements, 1946 nodes

Figure 5: Some meshes for the translating sphere benchmark.

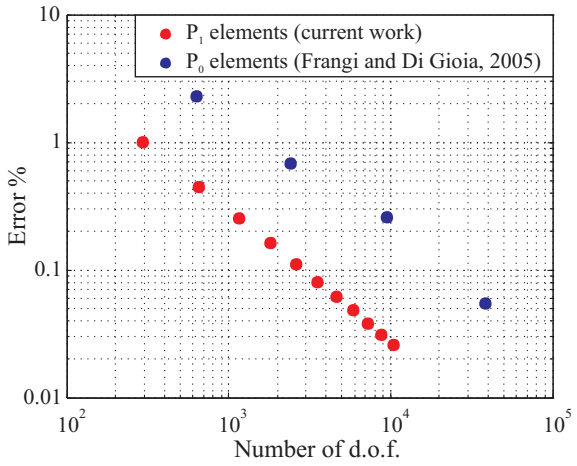

Figure 6: Numerical error for the translating sphere benchmark.

mm, width $b = 30\,\mu$m, height $h = 60\,\mu$m. In practice, this beam vibrates in vacuum. However, for the purposes of the present study, we will assume it vibrating in a air medium.

Let us discuss first the pertinence of the stationarity assumption applied to this case. Inertia forces can be neglected when compared to viscous forces when frequency of vibration ω is small enough, or equivalently, when the Reynolds number *Re* is much smaller than unity. If we take h as the characteristic dimension of the vibrating body, and introduce the penetration depth

$$\delta = \sqrt{\frac{2\mu}{\rho\omega}}, \tag{48}$$

we know that $Re \ll 1$ whenever $h/\delta \ll 1$ (Landau and Lifshitz, 1959).

Unfortunately, in this case, the frequency of the vibration mode (the one we are interested in) is $\omega = 4.45 \times 10^5$ s^{-1}, and hence $h/\delta = 7.30$, contradicting the initial stationary hypothesis. Then, we carry out an analysis where the frequency of the first mode of vibration of the given beam was decreased (by decreasing the Young modulus of the beam material) in order to decrease h/δ and detect the range of validity of the stationary hypothesis. Results are shown in Figure 8, where the numerically computed quality factor (Q_n) is compared to the analytical expression (Q_a) from Zhang and Turner (2007). The present numerical model always overestimate the quality factor. For current $h/\delta = 7.30$, Q_n is one order of magnitude higher than Q_a. Note however that $Q_n \to Q_a$ as $h/\delta \to 0$, validating the application of this model for low h/δ.

Anyway, the present problem involving high vibration frequencies can not be adequately

represented as a steady Stokes problem. The model proposed by Ding and Ye (2004) for oscillatory Stokes problems should provides a better approximation to high-frequency vibrating MEMS, and will be considered in future works.

Let us finally point out that the influence of deformation was found very small in this case: the computed quality factor differs 0.02% for models with and without deformation terms.

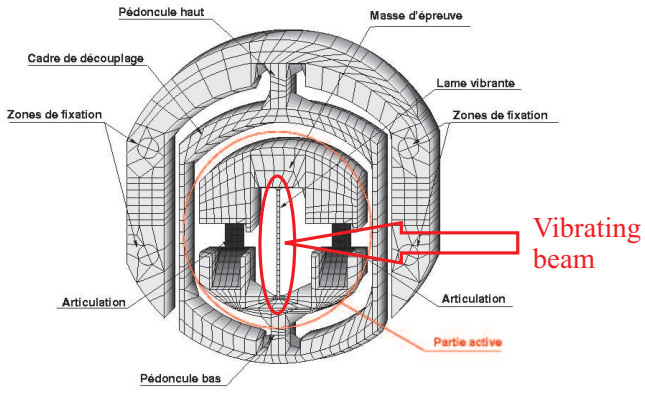

Figure 7: ONERA's VIA vibrating beam accelerometer.

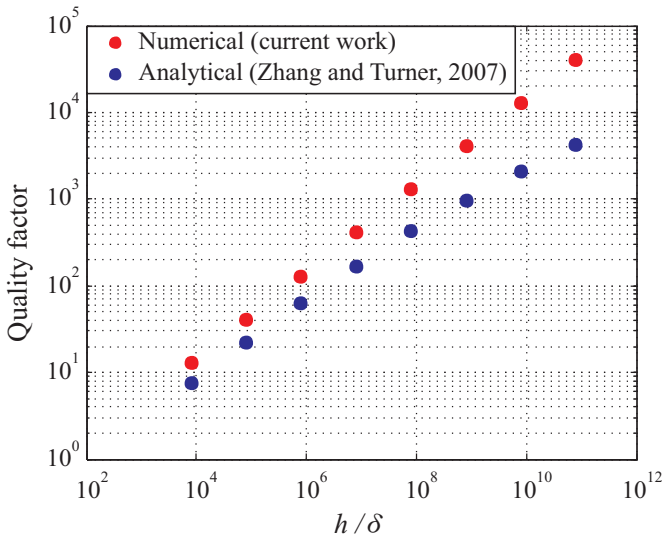

Figure 8: Numerically vs. analytically computed quality factor for the vibrating beam in ONERA's accelerometer.

8 CONCLUSIONS

We developed a boundary element method to solve the incompressible Stokes problem in general, and the exterior flow around MEMS in particular. We take into account the effect of MEMS deformation on fluid flow for the sake of generality, even though it seems to be negligible in practical applications. More studies are needed to support this observation in general MEMS applications. In any case, the present model is capable of simulating rigid-boundary problems with a satisfactory accuracy. In fact, the use of linear elements –richer that the constant elements commonly used– together with the analytical integration of singular terms –more accurate than numerical integration– contribute to improve the accuracy of the method.

Finally, despite the steady Stokes describes satisfactorily a large number of MEMS in practice were the Reynolds number is low enough, it is not the case with the VIA accelerometer we are particularly interested in. Future work will include the development of a model for oscillatory Stokes flow allowing to simulate MEMS vibrating at higher frequencies.

ACKNOWLEDGEMENTS

Financial support from ANPCyT, grant PAE 22592 Node 22961, and from Conicet, grant PIP 5271 is acknowledged.

REFERENCES

Blom F.R., Bouwstra S., Elwenspoek M., and Fluitman J.H.J. Dependence of the quality factor of micromachined silicon beam resonators on pressure and geometry. *J. Vac. Sci. Technol. B*, 10(1):19–26, 1992.

Ding J. and Ye W. A fast integral approach for drag force calculation due to oscillatory slip stokes flows. *Int. J. Numer. Meth. Engng.*, 60:1535–1567, 2004.

Frangi A. and Di Gioia A. Multipole BEM for the evaluation of damping forces on MEMS. *Comput Mech.*, 37:24–31, 2005.

Frangi A., Spinola G., and Vigna B. On the evaluation of damping in MEMS in the slipflow regime. *Int. J. Numer. Meth. Engng.*, 68(10):1031–1051, 2006.

Frangi A. and Tausch J. A qualocation enhanced approach for stokes flow problems with rigid-body boundary conditions. *Engineering Analysis with Boundary Elements*, 29:886–893, 2005.

Kim S. and Karrila S.J. *Microhydrodynamics: Principles and Selected Applications*. Butterworth-Heinemann, 1991.

Landau L.D. and Lifshitz E.M. *Fluid Mechanics*. Pergamon Press, 1959.

Le Traon O., Janiaud D., Muller S., and Bouniol P. The VIA vibrating beam accelerometer: Concept and performances. Proceedings of the Position, Location and Navigation Symposium. Palm Springs, USA, 1998.

Masson S. Finite element analysis using Oofelie: Piezo-thermo-elastic simulations for vibrating inertial sensors. X Samtech Users Conference 2007. Liège, Belgium, 2007.

Mukherjee S., Telukunta S., and Mukherjee Y.X. Bem modeling of damping forces on mems with thin plates. *Engineering Analysis with Boundary Elements*, 29:1000–1007, 2005.

París F. and Cañas J. *Boundary Element Method: Fundamentals and Applications*. Oxford University Press, 1997.

Power H. and Wrobel L.C. *Boundary Integral Methods in Fluid Mechanics*. Computational Mechanics Publications, 1995.

Wang X., Kanapka J., Ye W., Aluru N.R., and White J. Algorithms in FastStokes and its application to micromachined device simulation. *IEEE Transactions on Computer-Aided Design of Integrated Circuits and Systems*, 25(2):248–257, 2006.

Zhang W. and Turner K. Frequency dependent fluid damping of micro/nano flexural resonators: experiment, model and analysis. *Sensors and Actuators A*, 134:594–599, 2007.